Aust. J. Phys., 1978, **31**, 477–87

An Investigation of the Composition of a Hydrogen Plasma using Magnetoacoustic Oscillations

M. H. Brennan, B. L. Jessup and I. R. Jones

School of Physical Sciences, Flinders University of South Australia, Bedford Park, S.A. 5042.

Abstract

This paper reports on the use of observations of magnetoacoustic oscillations to determine the radial particle density and temperature profiles in a hydrogen plasma. The observations comprise measurements, at a number of frequencies, of the radial variations of the oscillation amplitude and of the total flux in the plasma. The analysis allows the determination of radial profiles of the ion and atom number densities.

1. Introduction

The use of magnetoacoustic oscillations as a plasma diagnostic technique has been investigated by a number of workers. A brief review of the different approaches adopted has been given by the present authors (Brennan *et al.* 1977) in a paper describing magnetoacoustic oscillations in an argon afterglow plasma. The general approach adopted by us in this earlier paper is followed here, and observations of the radial variations in the oscillation amplitude, and of the total flux in the plasma, are used to deduce radial profiles of density and temperature during and after the passage of an axial ionizing current in a hydrogen plasma.

Two important features distinguish the present work from our earlier work with an argon plasma. First, a single-turn loop surrounding the plasma, which provides a measure of the total flux in the plasma without causing perturbation, is shown to be capable of yielding data having an information content comparable with that of a magnetic probe. This is particularly important for hot dense plasmas where the use of a probe is precluded. Second, the constraint that the sum of the ion and atom densities should be constant and equal to the initial filling density, used in the previous argon work to determine the atom density for a given ion density distribution, has been removed. This was possible because the ion–atom collision frequencies in the present work are an order of magnitude greater than those for argon so that the atoms are sufficiently well coupled to the magnetoacoustic oscillations to allow the radial atom distribution to be accurately determined. Further, the analysis allows for the presence of molecules (not present, of course, in the case of argon).

In the present work, a careful choice of the parameterization of the density profiles allows the profiles to be unconstrained, except for the requirement that the densities are positive quantities and that there is no loss of particles from the discharge to the walls of the vessel—an assumption that is consistent with the results of a number of studies of similar discharges.

The theoretical model of the plasma, which closely follows the multifluid model of Jessup and McCarthy (1978), is briefly described in Section 2. The details of the experiment are given in Section 3. The results of the numerical analysis of the data, which yields the plasma density and temperature profiles, are presented in Section 4 and discussed in Section 5.

2. Theory

In the experiments described in Section 3, the plasma is contained in a cylindrical discharge vessel, of inner radius a, surrounded by a long coaxial solenoid of radius b ($b > a$). The plasma is embedded in a steady magnetic field B_0 directed along the axis of the discharge tube. An RF current passes through the solenoid, producing a magnetic field at the surface of the plasma which is given by

$$b_z(a,t) = \mathrm{Re}\{|b_z(a)|\exp(-\mathrm{i}\omega t)\}, \tag{1}$$

$|b_z(a)|$ being the amplitude of the field at $r = a$. It is assumed that the perturbation field is much smaller than the steady axial field, that is,

$$|b_z| \ll B_0 .$$

The plasma is described by a multifluid model with four particle species: ions, electrons, atoms and molecules (identified by the subscripts i, e, a, m). The number density of each of the species may vary with radius; quasi-neutrality is assumed, however, so that

$$n_\mathrm{i}(r) = n_\mathrm{e}(r) = n(r), \quad \text{say.}$$

For the experiments reported here, the energy equipartition times are all sufficiently small to allow the further assumption of equal ion, electron and atom temperatures:

$$T_\mathrm{i}(r) = T_\mathrm{e}(r) = T_\mathrm{a}(r) = T(r), \quad \text{say.}$$

For simplicity, we also extend the assumption of equal temperatures to the molecules ($T_\mathrm{m}(r) = T(r)$), even though this may not be valid in the outer regions of the plasma.

We follow Jessup and McCarthy (1978) and develop a model describing the plasma in terms of 12 linearized first-order equations of motion. These may be combined with Maxwell's equations and the equation relating the plasma current to the fluid velocities to yield a single second-order differential equation for the magnetic field $b_z(r)$ associated with the oscillation:

$$\frac{1}{r}\frac{\mathrm{d}}{\mathrm{d}r}\left(\frac{r}{\mu_0 M(r)}\frac{\mathrm{d}b_z}{\mathrm{d}r}\right) - \mathrm{i}\omega b_z = 0, \tag{2}$$

where $M(r)$ contains terms which include the particle masses, number densities and charges, the collision frequencies, B_0 and ω (Jessup 1977). Given $n(r)$, $n_\mathrm{a}(r)$, $n_\mathrm{m}(r)$, $T(r)$, the cross sections for momentum transfer, B_0 and ω, equation (2) can be solved numerically by the same technique as described by Frommelt and Jones (1975).

In general, $b_z(r)$ will be a complex quantity which can be written in the polar form

$$b_z(r,t) = \mathrm{Re}[|b_z(r)|\exp\{-\mathrm{i}(\omega t+\theta(r))\}], \tag{3}$$

where $|b_z(r)|$ and $\theta(r)$ are the amplitude and phase of b_z at radius r. The total flux $\phi(t)$ enclosed by a single loop of radius c ($a < c < b$) wound around the outside of the discharge vessel, but inside the exciting solenoid, is then given by

$$\phi(t) = \int_0^a 2\pi r\, b_z(r,t)\,\mathrm{d}r + \pi b_z(a,t)(c^2-a^2). \tag{4}$$

3. Experiment

(a) Plasma Generation

The experiments were carried out in a hydrogen plasma generated in the Flinders Plasma Source 2. The source consists of a 3 m long cylindrical Pyrex vacuum vessel of 5·2 cm inner radius. During the experiments hydrogen gas flowed continuously through the vessel, maintaining an equilibrium pressure of 200 mtorr (~26·6 Pa). A quasi-steady axial magnetic field B_0 was produced by discharging a capacitor bank through a solenoid surrounding the vacuum tube. Plasma generation and the excitation of magnetoacoustic oscillations occurred at a time close to that at which B_0 reached its peak value of 7·8 kG. Spatial and temporal variations in B_0 in the regions and times of interest did not exceed $\pm 3\%$.

The plasma was generated by means of a pulsed axial discharge of approximately 12 kA amplitude and 60 μs duration between a plane anode and a multipin cathode, of the type described by Müller *et al.* (1973), situated one at each end of the discharge tube.

A schematic diagram of the apparatus is shown in Fig. 1.

(b) Excitation of Magnetoacoustic Oscillations and their Detection

The magnetoacoustic oscillations were continuously excited by passing an RF current through a solenoid wound around the exterior of the discharge tube. The solenoid was 65 cm in length (i.e. six times the discharge tube diameter). Its centre was located 70 cm from the multipin cathode. The solenoid consisted of 20 coil units connected in parallel. Each unit incorporated a four-turn coil connected in series with a 1 kΩ resistor. The complete solenoid thus presented an impedance of 50 Ω to a 50 Ω low-power (~100 W) oscillator which provided RF current in the frequency range 1–5 MHz. This arrangement ensured that changes in oscillator output current arising from changes in the solenoid impedance due to plasma effects were small enough to be neglected. Typically, the amplitude of the vacuum magnetic perturbation field was 0·3 G (cf. B_0 = 7·8 kG).

Two methods were used to investigate the magnetoacoustic oscillations. The first entailed recording the unintegrated signal from a small probe inserted into a 4 mm o.d. quartz tube placed across a diameter of the discharge vessel in the midplane of the excitation solenoid. The probe could be located at any desired radial position and was oriented to detect the axial magnetic field component $b_z(r,t)$ of the oscillations. A frequency-independent measure of the amplitude of b_z was obtained by normalizing the amplitude of the probe signals obtained at various radial positions to the amplitude of the signal at the plasma boundary.

The second method involved recording the unintegrated output voltage from a single turn loop wound around the outside of the discharge tube and lying beneath the excitation solenoid at its midplane. Thus, for a given excitation frequency, the amplitude of the unintegrated signal from the loop was directly proportional to the total flux $\phi(t)$ defined by equation (4). Comparison of total fluxes at different frequencies was achieved by normalizing $\phi(t)$ to ϕ_v, the total flux without plasma.

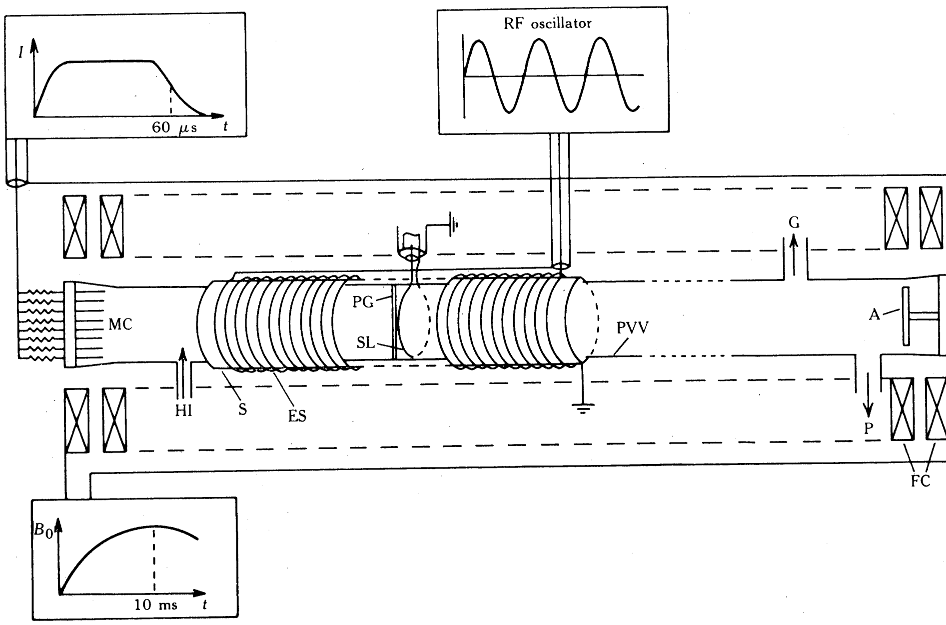

Fig. 1. Schematic diagram of the plasma source FPS 2. The abbreviations used are: A, anode; FC, axial magnetic field coils; P, pumps; G, gauges; PVV, Pyrex vacuum vessel; SL, single-turn loop; PG, probe guide; ES, excitation solenoid; S, electrostatic shield; HI, hydrogen inlet; MC, multipin cathode. In the insets, B_0 is the axial magnetic field, I is the plasma generation current and t is the time.

(*c*) *Experimental Results*

Results from the radial probe were obtained at frequencies of 1·5, 2·5, 3·5 and 4·5 MHz. At each frequency the variation of $|b_z(r)|$ with time was measured at 21 radial positions across the discharge vessel. Radial profiles of $|b_z(r)|$ at selected times in the afterglow plasma were constructed by cross-plotting the oscillogram traces of $|b_z(r,t)|$ for each frequency in turn. In Fig. 2 examples of such radial profiles obtained at $t = 100\ \mu s$ are shown (time is referred to the start of the ionizing current pulse). As indicated in subsection (*b*), the experimental data have been normalized to $|b_z(a)|$, the perturbation amplitude at the plasma boundary.

The data from the single loop were used to construct graphs of the normalized total flux $\phi(t)/\phi_v$ as a function of frequency for selected times in the lifetime of the plasma. By contrast with the radial probe, the signal from the loop was relatively free of noise generated by the ionizing current pulse, enabling measurements to be made during the ionizing current pulse. Data were obtained from the loop for 12 frequencies in the range 1–4·5 MHz so as to provide information of comparable content with that contained in the radial profiles obtained from the probe data. An example of the data obtained from the loop is shown in Fig. 3.

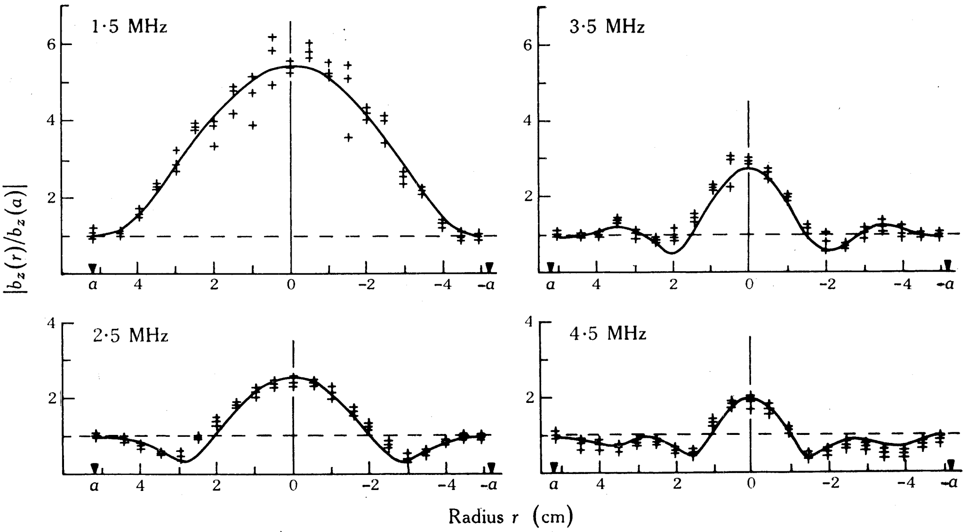

Fig. 2. Radial variation of $|b_z|$ at $t = 100\ \mu s$. The plotted points are the magnetic probe data and the curves are computed least-squares fits as described in Section 4.

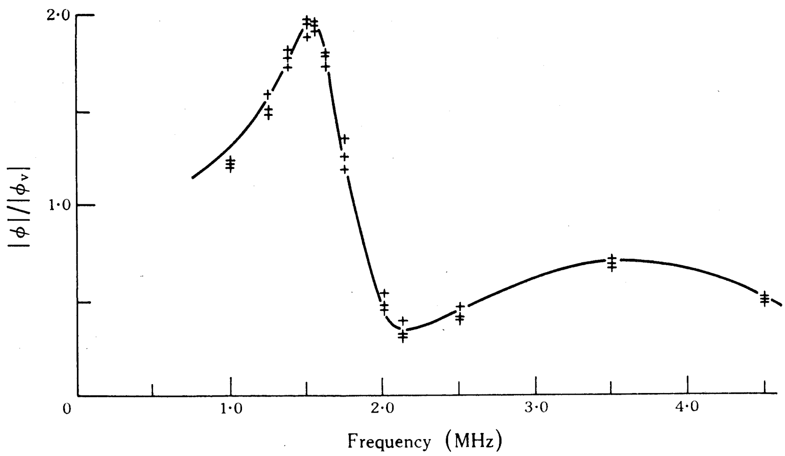

Fig. 3. Plot of the variation with frequency of the total magnetic flux ϕ detected by the single loop at $t = 100\ \mu s$. The flux is normalized at each frequency to the flux ϕ_v observed in the absence of plasma. The curve is a computed least-squares fit as described in Section 4.

4. Analysis of Experimental Data

(*a*) *Procedure*

The approach adopted in the analysis of the data obtained from the probe and the single-turn loop is generally similar to that used in our earlier study of an afterglow argon plasma (Brennan *et al.* 1977). There is, however, an important difference.

In the case of argon, there were only two particle number densities to be determined: the ions and the neutral atoms. It was reasonable to assume, and the results of the analysis supported the assumption, that the sum of the average ion and atom densities was constant in time and equal to the original filling number density.

The situation is more complex for the hydrogen discharge where there are three unknown number densities: ions, atoms and molecules. The results of a number of previous studies of similar discharges, including the work of Brown *et al.* (1966) and R. C. Cross and B. D. Blackwell (personal communication), suggest that there is no significant reduction in total average number density during such discharges. We therefore assume, for the purposes of the present analysis, that the average total number density n_T of ions, atoms and molecules (counted with a weight of two) is constant in time and equal to twice the filling number density n_F of molecules (corresponding to 200 mtorr):

$$n_T = \bar{n}_i + \bar{n}_a + 2\bar{n}_m = 2n_F, \tag{5}$$

where

$$\pi a^2 \bar{n}_{i,a,m} = \int_0^a n_{i,a,m}(r)\, 2\pi r\, dr.$$

Another difference in approach between the present work and that of Brennan *et al.* (1977) occurs in the functional form used to characterize the radial variation in number densities. Here, one has to compromise between a form which is not physically acceptable (for example, a function which does not admit small, but finite, ion densities and temperatures in the outer regions of the plasma) and a form which requires more parameters than justified by the information content of the experimental data. After some preliminary investigation of several alternatives we adopted, for the present analysis, the following forms:

$$n_i(r) = n_{i0}(1 + a_1 r^4) \qquad \text{for} \qquad a_1 > -a^{-4}, \tag{6a}$$

$$= n_{i0}\{1-(r/a)^4\}^{1+a_2} \qquad a_1 \leqslant -a^{-4}; \tag{6b}$$

$$T(r) = T_0(1 + b_1 r^4) \qquad \text{for} \qquad b_1 > -a^{-4}, \tag{7a}$$

$$= T_0\{1-(r/a)^4\}^{1+b_2} \qquad b_1 \leqslant -a^{-4}; \tag{7b}$$

where a is the inner radius of the plasma vessel, and the forms (6b) and (7b) are chosen when a_1 falls to the value of $-a^{-4}$, that is, when n_i or T falls to zero at the tube wall. The flexibility of the above functional forms ensures that the computed plasma temperature and ion number density profiles are not influenced by artificial constraints introduced by the assumed functional forms of the profiles.

The atom density profile is characterized by

$$n_a(r) = n_{a0}(1 + c_1 r^4) \tag{8}$$

and the molecular profile by

$$n_m(r) = n_{m0}(1 + d_1 r^4), \tag{9}$$

subject to the constraint imposed by equation (5).

There are thus a total of seven free parameters describing the particle density and temperature profiles: n_{i0}, a_1 (or a_2), T_0, b_1 (or b_2), n_{a0}, c_1 and n_{m0}, one of the parameters (d_1, say) being determined by equation (5). This compares with the eight free parameters employed by Brennan *et al.* (1977). There are no constraints placed on the choice of parameter values other than that the densities and temperatures be positive quantities.

With the plasma characterized by the expressions (6)–(9), equation (2) was integrated numerically for each time of interest and the parameters were evaluated by minimizing the sum of the square of the deviations of the computed values of $|b_z(r)|$ (or total flux ϕ) from the corresponding experimentally determined values. It is important to note that the sum was carried out, in each case, over all frequencies for which data were available.

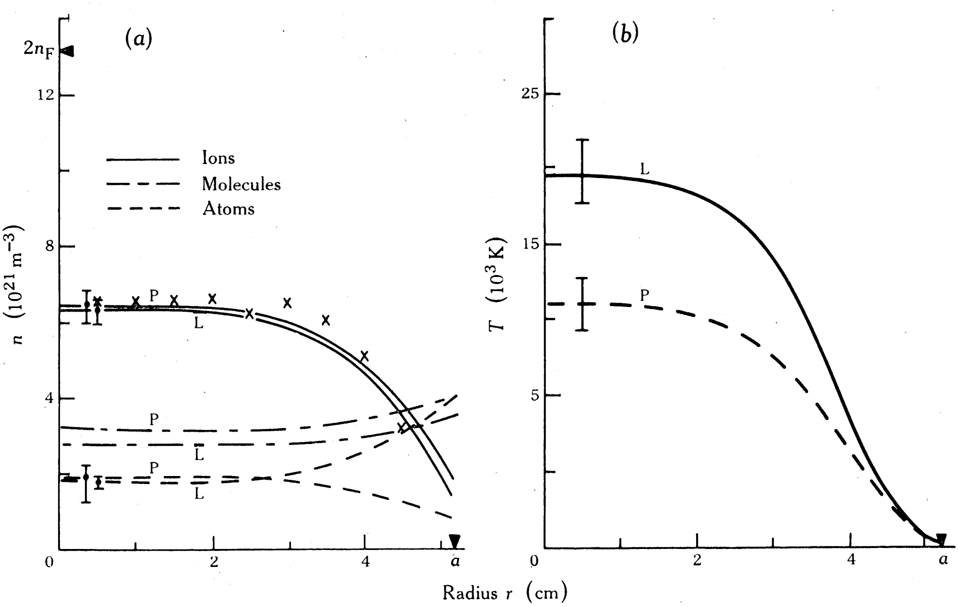

Fig. 4. Profiles of (*a*) number density n and (*b*) plasma temperature T corresponding to the computed least-squares fits to the probe (P) and loop (L) data shown in Figs 2 and 3. The crosses in (*a*) show the average electron number density obtained from laser interferometry.

Cross sections for momentum transfer between ions and atoms, which are required in such a procedure, were obtained from the published data of Fite *et al.* (1958), Dalgarno (1960), Belyaev *et al.* (1967) and Duman and Smirnov (1974). Accurate values for the ion–molecule and atom–molecule cross sections are not available. However, Cramer (1961) determined an upper limit of 1×10^{-20} m^2 for the charge exchange cross section for H^+–H_2 collisions at incident ion energies of 4–10 eV, while Belov (1966) calculated the exchange reaction cross section for H–H_2 collisions to be $1 \cdot 6 \times 10^{-20}$ m^2 at energies of 1 eV. Both these results are of the order of the geometric cross sections and are much less than the momentum transfer cross section for ion–atom collisions ($\sim 1 \times 10^{-18}$ m^2). We have therefore used geometric cross sections for both the ion–molecule and atom–molecule momentum transfer cross sections.

(b) Results

The results of applying the least-squares fitting procedure to the probe data at $t = 100\ \mu s$ are shown by the curves in Fig. 2. It is seen that an excellent fit to the observed $b_z(r)$ profiles is obtained at all four frequencies. The value of the usual fitting parameter χ^2, divided by the mean square experimental error (we use χ_n^2 for this 'normalized' value) is 2·2 in this case. It is interesting to note that if molecules are not assumed to be present or, equivalently, if the sum of the average ion and atom densities is required to be equal to the filling density, a very poor fit to the data is obtained, with $\chi_n^2 = 21$.

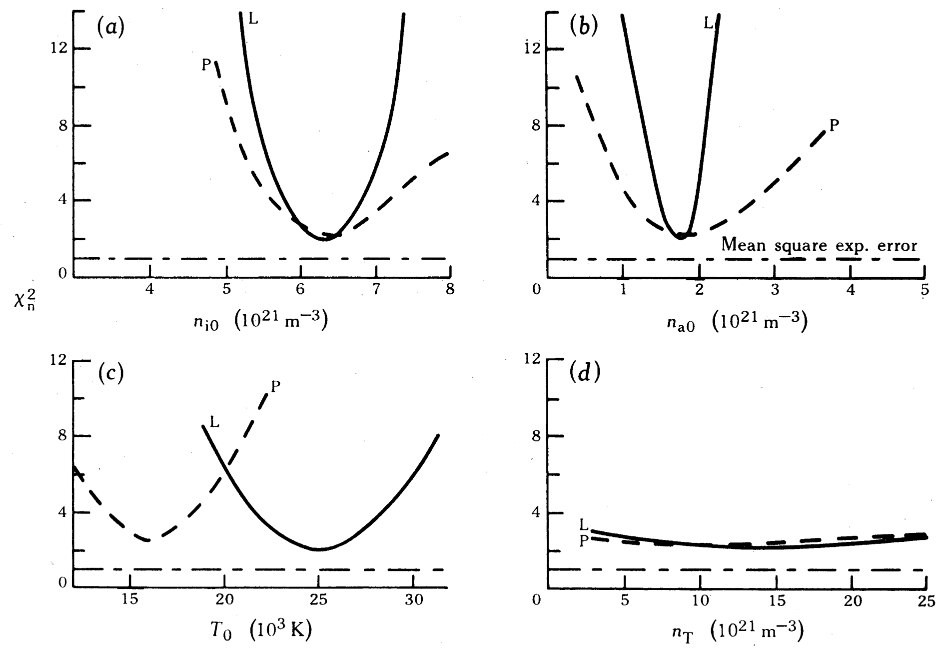

Fig. 5. Sensitivity of the normalized value of χ^2 to variations in (*a*) the assumed central ion number density n_{i0}, (*b*) the central atom number density n_{a0}, (*c*) the central temperature T_0 and (*d*) the average total number density n_T. The curves are results from the probe (P) and loop (L) data.

The results of the analysis for the data obtained with the single-turn loop are shown in Fig. 3. The value of χ_n^2 for this case is 2·0.

The density and temperature profiles required to obtain the least-squares fits of Figs 2 and 3 are shown in Figs 4*a* and 4*b*. Also shown in Fig. 4*a* is the electron density profile obtained by laser interferometry, as described by Brennan *et al.* (1977). No independent measurements of the atom or molecule profiles, or of the temperature profile, were attempted.

(c) Errors

The least-squares analysis yields values for eight parameters characterizing $n_i(r)$, $n_a(r)$, $n_m(r)$ and $T(r)$. In order to investigate the accuracy with which these profiles were determined, the data obtained at $t = 100\ \mu s$ were further analysed by holding all except one parameter fixed and calculating the variation in the value of χ_n^2 as that one parameter was varied about the value obtained by the least-squares fitting procedure. The four parameters chosen for this error analysis were the central ion number density n_{i0}, the central atom number density n_{a0}, the central plasma temperature T_0 and the average total number density n_T. The last quantity had been held fixed at twice the filling number density of molecules in the fitting procedure.

The results of the error analysis are presented in Fig. 5. These results were used to calculate the typical error bars of Fig. 4, where the error limits correspond to fits for which the computed curves are smooth fits to the extremes of the experimental error bars.

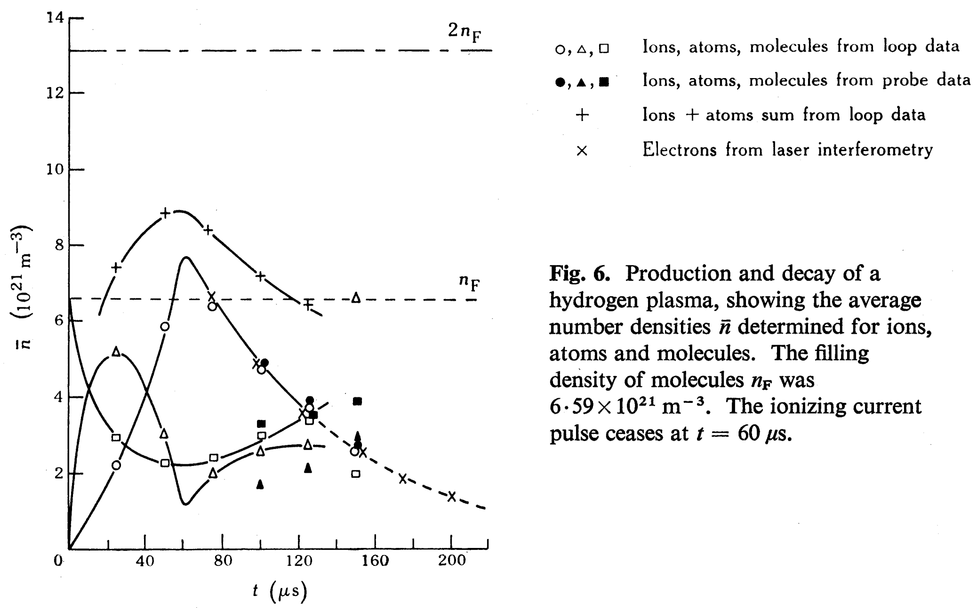

Fig. 6. Production and decay of a hydrogen plasma, showing the average number densities $\bar{n}$ determined for ions, atoms and molecules. The filling density of molecules n_F was $6 \cdot 59 \times 10^{21}$ m^{-3}. The ionizing current pulse ceases at $t = 60$ μs.

(*d*) *Evolution of Average Number Densities*

In addition to the analysis of the probe and loop data at $t = 100$ μs, similar analyses were made of the probe data at 125 and 150 μs and of the loop data at 25, 50, 75, 125 and 150 μs. The two earliest times for the loop data thus occurred before the end of the axial ionizing current pulse (at 60 μs). The theoretical work of Sy (1978) indicates that, for the conditions of the present experiment, the effects of the ionizing current on the characteristics of the magnetoacoustic oscillations can be ignored.

As indicated in Section 3*c*, noise from the ionizing current pulse precluded the use of probe data during the current pulse. Beyond $t \sim 150$ μs there was insufficient information content in the probe, or the loop, data to allow meaningful fits to be obtained between computed and observed $|b_z(r)|$ profiles, or the total flux ϕ. Indeed, significant discrepancies between the parameters deduced from the two sets of data occurred at $t = 150$ μs. The study of the characteristics of the plasma is thus confined to the range $t = 25$–125 μs.

Although detailed density and temperature profiles were calculated from the least-squares analysis for $t = 25$–125 μs in the production and decay of the plasma, we present here in Fig. 6 only the average number densities for ions, atoms and molecules.

The curves shown in the figure are intended merely to assist the reader in following the behaviour of each of the particle species. Also shown is the average density of ions plus atoms as determined by the single loop.

5. Discussion

(*a*) *Ion Density*

The results presented in Fig. 4*a* show the very good agreement between the ion density profile obtained from the analysis of observations of the magnetoacoustic oscillations and the profile obtained by laser interferometry. Indeed, good agreement was obtained at all times between the interferometer measurements and the densities derived from an analysis of the loop data. Somewhat poorer agreement was obtained with the densities derived from the probe data (although the average number densities were in good agreement, as shown in Fig. 6). The superiority of the loop over the probe can probably be attributed to the wider range of frequencies used, thus ensuring that the data were always available near the fundamental magneto-acoustic resonance frequency, where variations in the ion density profile have the greatest effect on the profile of the oscillation amplitude $|b_z(r)|$.

The evolution of the average ion density, shown in Fig. 6, indicates that the plasma reached a peak level of ionization of $\sim 60\%$ at the end of the ionizing current pulse.

(*b*) *Atom Density*

The results presented in Figs 4, 5 and 6 reveal that the central and average atom densities obtained from the loop and the probe data are in fair agreement. The total ion plus atom density, shown in Fig. 6, reaches a value of $\sim 70\%$ of the total number density of atoms present before the discharge (i.e. $2n_F$). This is in good agreement with the value of 60% obtained by Malein (1965) for the same quantity early in the afterglow of a 200 mtorr hydrogen discharge, which was generated by an axial discharge of similar energy per volume of plasma as in the present experiment.

(*c*) *Molecule Density*

The small ion–molecule and atom–molecule collision cross sections result in only a very weak coupling of the molecules to the magnetoacoustic oscillation. Consequently, the fits to the experimental data are insensitive to variations in the assumed profiles, and (even) average values, of the molecule number density. This insensitivity is illustrated in Fig. 5*d*, where the value of χ_n^2 is seen to be only very weakly dependent on the average total number density, and hence on the average number density of molecules (through equation 5).

The present analysis can therefore not be used to determine whether or not significant numbers of molecules were present in the afterglow plasma. However, the analysis does show that it is not necessary to invoke the assumption of a large loss of particles, as was done by Malein (1965) in his analysis of a similar discharge. In this respect, the present work is consistent with the results of Brown *et al.* (1966) and Cross and Blackwell (personal communication). It is of interest to note in this connection that R. B. Howell (personal communication) has found that most of the radiation emitted by *z*-pinch discharges in hydrogen can be attributed to radiation from molecular hydrogen.

(d) Temperature

As was the case in the analysis by Brennan *et al.* (1977) of magnetoacoustic oscillation data in an argon afterglow plasma, the temperature of the plasma is not well determined by the type of analysis employed here. It is possible that the addition of information about the phase of $b_z(r)$, or of the loop signal, with respect to the current flowing in the excitation solenoid (in a manner similar to that employed by Cross and Blackwell (personal communication) in their analysis of the impedance of such an excitation solenoid) may result in a more accurate determination of plasma temperature.

Acknowledgments

This work was supported by grants from the Australian Institute of Nuclear Science and Engineering and the Australian Research Grants Committee.

References

Belov, V. A. (1966). *Teplofiz. Vys. Temp.* **4**, 625.
Belyaev, V. A., Brezhnev, B. G., and Eratsov, E. M. (1967). *Sov. Phys. JETP* **25**, 777.
Brennan, M. H., Jessup, B. L., and Jones, I. R. (1977). *J. Plasma Phys.* **18**, 127.
Brown, I. G., Cross, R. C., James, B. W., and Watson-Munro, C. N. (1966). *Phys. Lett.* **23**, 451.
Cramer, W. H. (1961). *J. Chem. Phys.* **35**, 836.
Dalgarno, A. (1960). *Proc. Phys. Soc. London* **75**, 375.
Duman, E. L., and Smirnov, B. M. (1974). *High Temp. (USSR)* **12**, 431.
Fite, W. L., Brackman, R. T., and Snow, W. R. (1958). *Phys. Rev.* **112**, 1161.
Frommelt, J. J. B., and Jones, I. R. (1975). *J. Plasma Phys.* **14**, 373.
Jessup, B. L. (1977). Ph.D. Thesis, Flinders University.
Jessup, B. L., and McCarthy, A. L. (1978). *IEEE Trans. Plasma Sci.* **6**, 220.
Malein, A. (1965). *Nucl. Fusion* **5**, 352.
Müller, G., Räuchle, E., and Schüller, P. G. (1973). *Plasma Phys.* **15**, 925.
Sy, W. N-C. (1978). *Plasma Phys.* **20**, 33.

Manuscript received 7 November 1977